International Journal of Heat and Mass Transfer 91 (2015) 602–610

Contents lists available at ScienceDirect

International Journal of Heat and Mass Transfer

journal homepage: www.elsevier.com/locate/ijhmt

Temperature distribution in multi-layer skin tissue in presence of a tumor

Daipayan Sarkar, A. Haji-Sheikh, Ankur Jain *

Mechanical and Aerospace Engineering Department, The University of Texas at Arlington, Arlington, TX 76019, USA

ARTICLE INFO

Article history:
Received 9 February 2015
Received in revised form 21 July 2015
Accepted 22 July 2015

Keywords:
Bioheat transfer
Pennes equation
Multilayer tissue
Analytical solutions

ABSTRACT

Analytical investigation of bioheat transfer is of significant importance for numerous medical applications, for example in thermally-driven treatments for cancer. While bioheat transfer has been investigated for a number of specific conditions, relatively less work exists on bioheat transfer in a multilayer structure, such as skin. This paper presents an analytical solution for the steady-state Pennes bioheat equation in a multi-layer structure. The temperature distribution in each layer is derived separately and interface temperature and heat flux compatibility conditions are used to determine the complete solution. This solution is used to analyze the effect of heat generation during thermal therapy on a tumor in skin, which is modeled as a five-layer structure. The model is capable of accounting for the effects of various therapeutic measures such as cryotherapy, laser treatment, etc. as well as various physical phenomena such as conduction, blood perfusion and metabolism. The model is used to analyze the effect of various physical parameters on the temperature distribution. This theoretical treatment, as well as the quantitative results presented here may help improve the fundamental understanding of bioheat transfer in a layered structure such as skin.

© 2015 Elsevier Ltd. All rights reserved.

1. Introduction

Heat transport in tissues is an important physical phenomenon for both healthy and diseased tissue. A significant amount of research in bioheat transfer over the past few decades has led to an understanding of the governing dynamics of thermal transport in a tissue [1–3]. A number of thermal based therapeutic measures have been developed and adopted in practice, including laser surgery, cryotherapy, magnetic nanoparticle based hyperthermia and radio frequency ablation [4–9]. The design and optimization of these procedures has been aided by advancements in the understanding of bioheat transfer. Thermal transport in a biological system is sensitive to a number of critical parameters such as rate of metabolism, blood perfusion and space dependent heat generation in the presence of a tumor [2]. Hence, careful consideration should be given to all these properties and phenomena, when studying the nature of the temperature field in such systems.

Several models governing the flow of heat in tissues have been proposed. A classical model was presented by Pennes in 1948 [2], followed by several refinements and related models [3,10,11]. Detailed reviews of these bioheat transfer models are also available [12,13]. The Pennes model is used widely due to its simplicity, but it must be modified depending on unique attributes of the tissue under study. This model includes the effect of heat transfer in a biological body due to diffusion, advection, volumetric heat generation due to metabolism and spatial heating. Diffusion and transient thermal effects in any tissue are based on its thermophysical properties such as thermal conductivity, density and specific heat. The Pennes equation accounts for blood flow through an advection term, consisting of the thermophysical properties of blood along with the difference between the blood temperature and the local tissue temperature. Thermophysical properties of blood and various tissue have been measured using a variety of methods [14]. Some analytical work has been reported on solving the Pennes bioheat transfer equation for specific conditions. Deng et al. reported a closed form analytical solution for spatial and time dependent surface or volumetric conditions using the Green's function method [15]. Laplace transform was used to study the transient effects of sinusoidal heat flux on a one-dimensional semi-infinite tissue [4]. Mahjoob and Vafai developed an analytical model for a biological tissue, assuming a porous media with contributions due to conduction between tissue and vascular system, convective heat transfer between blood and tissue, heat generation due to metabolism and induced surface heat flux [16]. A dual layer biological media was also considered, and analytical solutions for

* Corresponding author. Tel.: +1 817 272 9338; fax: +1 817 272 2952.
E-mail address: jaina@uta.edu (A. Jain).

http://dx.doi.org/10.1016/j.ijheatmasstransfer.2015.07.089
0017-9310/© 2015 Elsevier Ltd. All rights reserved.

Nomenclature

a	length of tissue, m
b	location of each interface from datum, m
c	specific heat of blood, J/kg-K
C	series coefficient used in all sections
d	thickness of layer, m
D	series coefficient used in a solution for case in Section 2.2
g	volumetric heat generation, W/m^3
h	heat transfer coefficient, W/m^2-K
k	thermal conductivity, W/m-K
L	length of tumor region, m
m	parameter defined in Eq. (2)
q	heat flux, W/m^2
Q	heat transfer in resistor network, W
T	temperature, °C
x	spatial co-ordinate, m
y	spatial co-ordinate, m
β	eigen value in y, m^{-1}
γ	eigen value in x, m^{-1}
δ	factor to determine location of tumor
Φ	source term used in a solution for case in Section 2.2
Ψ	source term used in all solutions
Z	set of integers

Subscripts/superscripts

bl	blood
f	effect of flux boundary condition in superimposed solution
j	layer
n	number of terms
p	number of terms
r	resistor network solution
s	effect of source in superimposed solution
t	tumor region
sur	surface
∞	ambient
$*$	set of integers (Z) including zero, {0,1,2,3,…}
$+$	set of integers (Z) excluding zero, {1,2,3,…}

two specific cases were discussed [17]. An analytical study of an axisymmetric tissue-vascular system is used to analyze the effect due to the radiofrequency ablation treatment due to volumetric heat generation in the tissue region due to a heater probe [9]. The application of Pennes equation to magnetic fluid hyperthermia has been studied, where a theoretical solution is presented for a spherical tumor surrounded by a thin shell of magnetic nanoparticles [7]. An analytical model was proposed to investigate the rate of cell destruction during a freeze–thaw cryosurgical procedure, in order to minimize damage to healthy cells [5]. Steady state temperature distribution in a one dimensional cylindrical tissue has been developed for human limbs [18]. Steady state thermal penetration depth has been derived analytically using method based on Laplace transforms [19]. Analytical solution based on the Laplace transforms is used to solve a two-dimensional Pennes bioheat equation for both Fourier and non-Fourier heat conduction effects for a cylindrical skin tissue [20].

In addition to such analytical models, numerical solutions have also been developed for scenarios where temperature solutions are difficult to determine explicitly. Steady state temperature in breast cancer was studied numerically through user-defined functions to account for blood perfusion and metabolism [21]. An investigation of minimum invasive methods such as microwave thermal therapy was performed both numerically and experimentally, *in vivo* and *in vitro*, to determine the extent of the tissue injury [22]. Temperature solution in a system with time-dependent spatial heating has been studied numerically [23]. The cooling of human brain and neck in emergency medical situations has been studied using finite element simulations [24]. In a recent finite element based analysis, an alternating magnetic field is applied to ferrofluids to generate heat inside a tumor. The Pennes bioheat equation was coupled with Maxwell's equation in the finite element model to calculate the input parameters such as the magnetic flux intensity [25]. A finite difference model of the Pennes bioheat equation was used to study the effects of cryofreezing using the immersed boundary method [26]. Skin surface cooling based on optical window contact cooling, cryogenic spray cooling are considered for the Pennes bioheat equation and Weinbaum–Jiji bioheat model. Combined conduction and radiation effects are considered in Pennes equation and the temperature field in the multilayer tissue structure is computed numerically [27].

Finally, a number of experimental investigations of bioheat transfer in tissue have also been reported. The different theories involved with hyperthermia treatment were verified by performing experiments on a large bovine kidney by turning it into tissue phantom using alcohol fixation technique [28]. Most of these papers investigate therapy of cancerous tissue, including electroporation-based chemotherapy [6,29,30], magnetic nanoparticle based heating [7,8], etc. In a recent study, a high resolution microcomputed tomography imaging system has been used to investigate the concentration and distribution of injected nanoparticles. Also nanoparticle induced volumetric heat generation rate was measured experimentally [8]. Several studies on estimating the thermal damage potential due to Joule heating and the importance of considering the multilayer nature of skin tissue have also been presented [6,31,32]. In a related work, detection of shape, size and depth of a melanoma lesion by applying a cold stimulus at the surface has been reported [33]. In addition, an extension to Pennes bioheat equation is made to include the effect of water evaporation during in the tissue during laser heating. A source term is added to the Pennes bioheat equation to account for the energy required for evaporation process to occur, based on which, a relationship for effective specific heat is derived. Experiments on a liver tissue along with numerical solutions are presented to illustrate the effect of water evaporation from the tissue [34].

Techniques for temperature field computation during such procedures continue to be critical for design and optimization of present and future therapies. Unique bioheat transfer phenomena may be expected in skin due to its unique multi-layer structure and the resulting heterogeneity in thermophysical properties and biotransport parameters in the transverse direction. Recognition of the multi-layer nature of the skin – and the resulting bioheat transfer characteristics – is important for analyzing thermal effects in the presence of, and in treating skin lesions and cancers. While some work has been presented in understanding bioheat transfer in skin [4,13], the present literature lacks analytical solutions of Pennes bioheat equation for a multilayer structure. Analytical solutions for multilayer structures have been proposed for other engineering applications [35–38], however, bioheat transfer in a multilayer structure presents additional challenges due to the complicated nature of the governing equation. This paper presents the

Table 1
Geometrical parameters and thermophysical properties of various materials. Thermal conductivity and blood perfusion rate of tumor is assumed to be the same as papillary dermis.

Region	Thermal conductivity (W/m-K)	Blood perfusion ($m^3/s/m^3$)	Heat generation (W/m^3)	Distance from datum (m)
Muscle	0.51 [43]	0.0027 [43]	684.2 [43]	0.0025 [43]
Fat	0.185 [43]	0.00008 [43]	368.3 [43]	0.0075 [43]
Reticular dermis	0.445 [43]	0.00126 [43]	368.1 [43]	0.009 [43]
Papillary dermis	0.445 [43]	0.00018 [43]	368.1 [43]	0.01 [43]
Epidermis	0.235 [43]	0 [43]	0 [43]	0.011 [43]
Tumor	0.445	0.00018	500000 [8]	0.01

Blood: Density = 1060 kg/m^3 [43], heat capacity = 3770 J/kg-K [43].
Length of the tissue (a) = 0.05 m.

analytical derivation of temperature distribution for a two-dimensional, five layer skin tissue in the presence of a tumor. The Pennes bioheat equation is solved analytically for a multilayer geometry with varying thermal properties and biotransport parameters in the layers. Modeling the reaction term presents an additional challenge in the analytical framework since the blood perfusion rate varies in different layers of the tissue. Further, it is found that the analytical treatment needs to be modified significantly depending on the nature of the boundary condition on top of the skin structure. In addition to different physical boundary conditions and the reaction term, the analytical solution also includes the effect of metabolism in every layer of the skin tissue as a volumetric source and a spatially dependent source term representing the tumor. Results are found to be in good agreement with finite-element simulations. The analytical model is used for understanding the thermal effect of heat generation in a tumor in one of the skin layers. The effect of various thermophysical and geometrical parameters is studied. Results presented here may help improve the understanding of thermal transport in multi-layered tissue such as skin, and in particular contribute towards effective thermal-based therapies for skin cancers.

2. Mathematical model

In this section, the mathematical derivation of temperature distributions in a multilayer biological body is discussed. Consider the geometry of a five-layer skin tissue shown schematically in Fig. 1. Numerical values for various geometrical parameters and thermophysical properties of the various tissue layers are listed in Table 1. Consider the presence of a tumor of a given size in one of the layers. Heat generation in the tumor, as well as boundary conditions of the top and bottom surfaces result in a temperature field in the multilayer tissue. In order to determine this temperature field analytically, the governing Pennes bioheat equation for each layer is solved separately, accounting for temperature and heat flux compatibility at the interfaces between adjacent layers. Solutions are derived for three specific boundary conditions. This analysis does not consider the effect of evaporation, since the Pennes bioheat equation does not account for this phenomena and suitable modifications need to made either in governing equation or surface condition of the boundary value problem [34,39]. While the governing equation remains the same for each case, algebraic modifications to the source term in the governing equation are needed to capture the effect of various terms. The governing energy equation the temperature distribution $T_j(x, y)$ for each layer j is given by:

$$\frac{\partial^2 T_j}{\partial x^2} + \frac{\partial^2 T_j}{\partial y^2} - m_j^2 (T_j - T_{bl}) + \frac{g_{m,j}}{k_j} + \delta_j \frac{g_{t,j}(y)}{k_j} = 0 \tag{1}$$

where,

$$m_j^2 = \frac{w_j \rho_{bl} c_{bl}}{k_j} \tag{2}$$

In Eq. (1), $g_{m,j}$ refers to the volumetric heat generation inside a tissue due to metabolism and $g_{t,j}(y)$ refers to inherent heat generation in the tumor and/or heat generation due to targeted thermal therapy in the tumor region. The factor δ_j is introduced to represent the presence or absence of the tumor in the jth layer. w_j, ρ_{bl}, c_{bl} and k_j refer to blood perfusion rate, density of blood, specific heat of blood and thermal conductivity of tissue. The core of the skin tissue is held at a constant temperature of T_{bl} = 37 °C, and side walls are assumed to be adiabatic.

$$T_1 = T_{bl} \quad \text{at } x = 0 \tag{3}$$

$$\frac{\partial T_j}{\partial y} = 0 \quad \text{at } y = 0, a \tag{4}$$

Due to the multilayer nature of the problem, additional equations are obtained from compatibility at the interface between adjacent layers. Assuming perfect thermal contact,

$$T_j = T_{j+1} \quad \text{at } x = b_j, \quad j = \{1, 2, 3, 4\} \tag{5}$$

$$k_j \frac{\partial T_j}{\partial y} = k_{j+1} \frac{\partial T_{j+1}}{\partial y} \quad \text{at } x = b_j, \quad j = \{1, 2, 3, 4\} \tag{6}$$

Three specific boundary conditions that model various physical phenomena at the top of the skin are considered next.

2.1. Temperature prescribed at the top surface of skin tissue

This sub-section considers the case where a prescribed temperature is applied at the top surface of the skin tissue.

$$T_5 = T_{sur} \quad \text{at } x = b_5 \tag{7}$$

The solution to Eqs. (1)–(7) can be obtained by the following superposition technique,

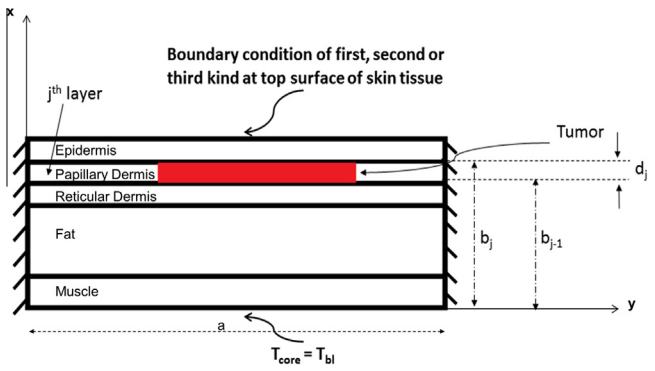

Fig. 1. Geometry of the multi-layer biothermal transport problem considered in this paper.

$$T_j(x,y) = T_{j,r}(x) + T_{j,s}(x,y) \tag{8}$$

The above superposition technique is chosen in order to account for the non-homogeneities in Eqs. (1), (3) and (7). $T_{j,r}(x)$ is the resistor network solution which accounts for the non-homogeneities in Eqs. (3) and (7) with the governing equation being homogeneous. $T_{j,s}(x,y)$ refers to the solution due to the contribution of source terms in each layer as observed in the governing equation with all boundary conditions being homogeneous. Substituting Eq. (8) in the governing Eqs. (1)–(7) results in the following set of equations for $T_{j,r}(x)$:

$$\frac{d^2T_{j,r}}{dx^2} = 0 \tag{9a}$$

$$T_{1,r} = T_{bl} \quad \text{at } x = 0 \tag{9b}$$

$$T_{5,r} = T_{sur} \quad \text{at } x = b_5 \tag{9c}$$

Similarly the $T_{j,s}(x,y)$ problem is given by:

$$\frac{\partial^2T_{j,s}}{\partial x^2} + \frac{\partial^2T_{j,s}}{\partial y^2} - m_j^2T_{j,s} + \frac{g_{m,j}}{k_j} + \delta_j\frac{g_{t,j}(y)}{k_j} + m_j^2T_{j,bl} - m_j^2T_{j,r}(x) = 0 \tag{10a}$$

$$T_{1,r} = T_{bl} \quad \text{at } x = 0 \tag{10b}$$

$$T_{1,s} = 0 \quad \text{at } x = 0 \tag{10c}$$

$$T_{5,r} = T_{sur} \quad \text{at } x = b_5 \tag{10d}$$

$$T_{5,s} = 0 \quad \text{at } x = b_5 \tag{10e}$$

$$\frac{\partial T_{j,s}}{\partial y} = 0 \quad \text{at } y = 0 \text{ and } y = a \tag{10f}$$

Note that both $T_{j,r}(x)$ and $T_{j,s}(x,y)$ follow interface compatibility equations similar to Eqs. (5) and (6). The solution for $T_{j,r}(x)$ is obtained using resistor network analogy [40] as follows:

$$T_{j,r}(x) = T_{j-1,r}(b_{j-1}) + Q\frac{(x-b_{j-1})}{ak_j} \tag{11}$$

where j = 1–5 and b_0 = 0

$$Q = \frac{T_{sur} - T_{bl}}{\left(\sum_{j=1}^{5}\frac{d_j}{k_j}\right)} \tag{12}$$

where $d_j = b_j - b_{j-1}$

The solution for $T_{j,s}(x,y)$ is obtained using the method of separation of variables, starting with a general transformation,

$$T_{j,s}(x,y) = \sum_{n=0}^{\infty}\sum_{p=1}^{\infty}C_{np}X_{p,j,s}(x)Y_{n,j,s}(y) \tag{13}$$

$$\Psi_{j,s}(x,y) = \frac{g_{m,j}}{k_j} + \delta_j\frac{g_{t,j}(y)}{k_j} + m_j^2T_{j,bl} - m_j^2T_{j,r}(x) \tag{14}$$

Substituting Eqs. (13) and (14) into Eq. (10a) results in

$$\sum_{n=0}^{\infty}\sum_{p=1}^{\infty}C_{np}(\gamma_p^2 + \beta_n^2 + m_j^2)X_{p,j,s}(x)Y_{n,j,s}(y) = \Psi_{j,s}(x,y) \tag{15}$$

where γ_p and β_n are the eigenvalues. The respective ordinary differential equations in X and Y are given by,

$$\frac{X''_{j,s}(x)}{X_{j,s}(x)} = -\gamma_p^2 \qquad \forall p \in Z^+ \tag{16}$$

$$\frac{Y''_{j,s}(y)}{Y_{j,s}(y)} = -\beta_n^2 \qquad \forall n \in Z^+ \tag{17}$$

Solutions to Eqs. (16) and (17) are obtained as follows [35]:

$$X_{j,s}(x) = A_{j,s}\cos(\gamma_p(x - b_{j-1})) + B_{j,s}\sin(\gamma_p(x - b_{j-1})) \tag{18}$$

$$Y_{j,s}(y) \approx \cos(\beta_n y), \quad \beta_n = \frac{n\pi}{a} \quad \forall n \in Z^* \tag{19}$$

The coefficients in Eq. (18) are obtained by using the compatibility condition at the interface of adjacent layers. The coefficients are found out to be governed by recursive relations [35],

$$A_{j+1,s} = A_{j,s}\cos(\gamma_p d_j) + B_{j,s}\sin(\gamma_p d_j), \quad j = \{1,2,3,4\} \tag{20a}$$

$$B_{j+1,s} = \frac{k_j}{k_{j+1}}[-A_{j,s}\sin(\gamma_p d_j) + B_{j,s}\cos(\gamma_p d_j)], \quad j = \{1,2,3,4\} \tag{20b}$$

where the coefficient $A_{1,s}$ is zero. $B_{1,s}$, which can be selected as any constant, is taken as 1. The final step is to determine the series coefficients in Eq. (15) using the orthogonality principle [41,42]:

$$C_{np} = \frac{\sum_{j=1}^{5}\int_{y=0}^{a}\left(\int_{x=b_{j-1}}^{b_j}k_j\frac{\Psi_{j,s}(x,y)X_{p,j,s}(x)}{(\gamma_p^2+\beta_n^2+m_j^2)}dx\right)Y_{n,j,s}(y)dy}{N_xN_y} \tag{21}$$

where, the respective norm integrals N_x and N_y are calculated as,

$$N_x = \sum_{j=1}^{5}\int_{b_{j-1}}^{b_j}k_jX_{p,j}^2(x)dx \tag{22}$$

$$N_y = \int_0^a Y_{n,j}^2(y)dy \tag{23}$$

An expression for the final solution for case 2.1 is obtained by adding the two solutions,

$$T_j(x,y) = T_{j-1,r}(b_{j-1}) + \frac{(T_{sur}-T_{bl})(x-b_{j-1})}{ak_j\left(\sum_{j=1}^{5}d_j/k_j\right)} + \sum_{n=0}^{\infty}\sum_{p=1}^{\infty}\frac{\sum_{j=1}^{5}\int_{y=0}^{a}\left(\int_{x=b_{j-1}}^{b_j}\frac{k_j\Psi_{j,s}(x,y)X_{p,j,s}(x)dx}{(\gamma_p^2+\beta_n^2+m_j^2)}\right)Y_{n,j,s}(y)dy}{N_xN_y}X_{p,j,s}(x)Y_{n,j,s}(y) \tag{24}$$

2.2. Heat flux prescribed at the top surface of skin tissue

The second case considers a prescribed heat flux applied at the top surface of the skin tissue. The governing equations for this case are given by Eqs. (1), (3) and (4), similar to case 2.1. In addition, Eq. (7) in Section 2.1 is replaced by,

$$k_5\frac{\partial T_5}{\partial x}\bigg|_{x=b_5} = q_{sur}(y) \tag{25}$$

The solution procedure for Eqs. (1)–(6) and (25) proceeds along similar lines as the solution in Section 2.1. However an additional transformation is needed, wherein the core body temperature T_{bl} is subtracted out from the temperature distribution:

$$\tilde{T}_j(x,y) = T_j(x,y) - T_{bl} \tag{26}$$

This results in the following equations for $\tilde{T}_j(x,y)$:

$$\frac{\partial^2\tilde{T}_j}{\partial x^2} + \frac{\partial^2\tilde{T}_j}{\partial y^2} - m_j^2\tilde{T}_j + \frac{g_{m,j}}{k_j} + \delta_j\frac{g_{t,j}(y)}{k_j} = 0 \tag{27}$$

$$\tilde{T}_1 = 0 \quad \text{at } x = 0 \tag{28}$$

$$\frac{\partial\tilde{T}_j}{\partial y} = 0 \quad \text{at } y = 0 \text{ and } y = a \tag{29}$$

$$\left.\frac{\partial \tilde{T}_5}{\partial x}\right|_{x=b_5} = q_{sur}(y)/k_5 \tag{30}$$

Similar to the previous sub-section, $\tilde{T}_j(x,y)$ is split into two components to account for the two non-homogeneities in the governing equations

$$\tilde{T}_j(x,y) = \tilde{T}_{j,f}(x,y) + \tilde{T}_{j,s}(x,y) \tag{31}$$

In Eq. (31), $\tilde{T}_{j,f}(x,y)$ accounts for non-homogeneity in the boundary condition, Eq. (30) and $\tilde{T}_{j,s}(x,y)$ accounts for non-homogeneity in the governing equation, Eq. (27). Inserting Eq. (31) in Eq. (27) we obtain the following set of equations given by,

$$\frac{\partial^2 \tilde{T}_{j,f}}{\partial x^2} + \frac{\partial^2 \tilde{T}_{j,f}}{\partial y^2} - m_j^2 \tilde{T}_{j,f} = 0 \tag{32a}$$

$$\frac{\partial^2 \tilde{T}_{j,s}}{\partial x^2} + \frac{\partial^2 \tilde{T}_{j,s}}{\partial y^2} - m_j^2 \tilde{T}_{j,s} + \frac{g_{m,j}}{k_j} + \delta_j \frac{g_{t,j}(y)}{k_j} = 0 \tag{32b}$$

$\tilde{T}_{j,s}(x,y)$ can be determined using a procedure similar to $T_{j,s}(x,y)$ in the previous section, with a minor change in the value of the coefficients. $\tilde{T}_{j,f}(x,y)$ presents additional difficulty as discussed below. This derivation starts with the transformation

$$\tilde{T}_{j,f}(x,y) = \sum_{n=0}^{\infty} D_n \tilde{X}_{n,j,f}(x) Y_{n,j} \tag{33}$$

Substituting Eq. (33) in Eq. (32a) results in

$$\frac{\tilde{X}''_{n,j,f}(x)}{\tilde{X}_{n,j,f}(x)} + \frac{Y''_{n,j}(y)}{Y_{n,j}(y)} - m_j^2 = 0 \qquad \forall\, n \in Z^* \tag{34}$$

$\tilde{X}_j(x,y)$ and $Y_j(x,y)$ can be separated as follows:

$$\frac{Y''_j(y)}{Y_j(y)} = -\beta_n^2 \qquad \forall\, n \in Z^* \tag{35}$$

and

$$\frac{\tilde{X}''_{j,f}(x)}{\tilde{X}_{j,f}(x)} = \beta_n^2 + m_j^2 = \eta_n^2 \qquad \forall\, n \in Z^* \tag{36}$$

Solution to the differential Eqs. (35) and (36) are given by,

$$Y_j(y) \approx \cos(\beta_n y), \quad \beta_n = \frac{n\pi}{a} \qquad \forall\, n \in Z^* \tag{37}$$

$$\tilde{X}_{n,j,f}(x) = E_{n,j,f}\cosh(\eta_n(x - b_{j-1})) + F_{n,j,f}\sinh(\eta_n(x - b_{j-1})) \quad \forall n \in Z^* \tag{38}$$

Note that in the special case of $m_j = 0$, i.e., zero blood perfusion rate in layer j, η_n in Eq. (36) becomes zero for $n = 0$. As a result, for $m_j = 0$ and $n = 0$, $\tilde{X}_{n,j,f}(x)$ is given by the following expression instead of Eq. (38),

$$\tilde{X}_{0,j,f}(x) = E_{0,j,f}(x - b_{j-1}) + F_{0,j,f}; \quad m_j = 0; \quad n = 0 \tag{39}$$

In this specific case, this scenario is encountered for the epidermis layer ($m_5 = 0$) due to zero perfusion rate of blood in that layer [43]. Heat flux and temperature compatibility at the interfaces are used to derive expressions for the coefficients in Eqs. (38) and (39):

$$\begin{aligned} &E_{n,j+1,f} = E_{n,j,f}\cosh(\eta_n d_j) + F_{n,j,f}\sinh(\eta_n d_j); \\ &j = \{1,2,3,4\}; \quad n \neq 0, \quad m_j \neq 0 \\ &F_{n,j+1,f} = \left(\frac{k_j}{k_{j+1}}\right)\left(\frac{m_j}{m_{j+1}}\right)[E_{n,j,f}\sinh(\eta_n d_j) + F_{n,j,f}\cos(\eta_n d_j)]; \\ &j = \{1,2,3,4\}; \quad n \neq 0, \quad m_j \neq 0 \end{aligned} \tag{40a}$$

Note that for the epidermis layer, where $m_5 = 0$, the coefficients corresponding to $n = 0$ are given by

$$\begin{aligned} &E_{0,5,f} = \left(\frac{k_4}{k_5}\right) m_4[E_{0,4,f}\sinh(m_4 d_4) + F_{0,4,f}\cosh(m_4 d_4)]; \quad n = 0; \quad m_5 = 0 \\ &F_{0,5,f} = E_{0,4,f}\sinh(m_4 d_4) + F_{0,4,f}\cosh(m_4 d_4); \quad n = 0; \quad m_5 = 0 \end{aligned} \tag{40b}$$

Similar to Section 2.1, the coefficients $E_{n,1,f}$ are zero, whereas the coefficients $F_{n,1,f}$, which could be chosen to be any constant are selected to be 1. The final step is to determine the series coefficients in Eq. (33), a procedure similar to Section 2.1. On substituting Eq. (33) into Eq. (32a) and then using orthogonality theorem, the series coefficients are obtained as

$$D_0 = \frac{\int_{y=0}^{a} q_{sur}(y)dy}{k_5 E_{0,5,f}}, \quad n = 0 \tag{41a}$$

$$D_n = \frac{\int_{y=0}^{a} q_{sur}(y) Y_{n,j}(y)dy}{k_5 \tilde{X}'_{n,j,f}(b_5) N_y} \quad \forall\, n \in Z^+ \tag{41b}$$

Following a procedure similar to Section 2.1 for the $T_{j,s}(x,y)$ solution, the temperature solution for the governing equation represented by Eq. (32b) for all homogeneous boundary conditions is given by,

$$\tilde{T}_{j,s}(x,y) = \sum_{n=0}^{\infty}\sum_{p=1}^{\infty} \frac{\sum_{j=1}^{5}\int_{y=0}^{a}\left(\int_{x=b_{j-1}}^{b_j} \frac{k_j \Phi_{j,s}(y) X_{p,j,s}(x)dx}{(\gamma_p^2 + \beta_n^2 + m_j^2)}\right) Y_{n,j,s}(y)dy}{N_x N_y} X_{p,j,s}(x) Y_{n,j,s}(y) \tag{42}$$

where, the norm integrals are similar to the integrals in Eqs. (22) and (23) and the source term is given by,

$$\Phi_{j,s}(y) = \frac{g_{m,j}}{k_j} + \delta_j \frac{g_{t,j}(y)}{k_j} \tag{43}$$

The final temperature solution for the prescribed heat flux boundary condition at the surface of the skin tissue is given by the following expression,

$$\begin{aligned} T_j(x,y) = T_{bl} &+ \left(\frac{\int_{y=0}^{a} q_{sur}(y)dy}{k_5 E_{0,5,f}} \tilde{X}_{0,j,f}(x)\right) \\ &+ \sum_{n=1}^{\infty} \frac{\int_{y=0}^{a} q_{sur}(y) Y_{n,j}(y)dy}{\tilde{X}'_{n,j,f}(b_5) N_y} \tilde{X}_{n,j,f}(b_5) Y_{n,j}(y) \\ &+ \sum_{n=0}^{\infty}\sum_{p=1}^{\infty} \frac{\sum_{j=1}^{5}\int_{y=0}^{a}\left(\int_{x=b_{j-1}}^{b_j} \frac{k_j \Phi_{j,s}(y) X_{p,j,s}(x)dx}{(\gamma_p^2 + \beta_n^2 + m_j^2)}\right) Y_{n,j,s}(y)dy}{N_x N_y} X_{p,j,s}(x) Y_{n,j,s}(y) \end{aligned} \tag{44}$$

2.3. Convective cooling at the top surface of skin tissue

The third scenario considered here involves convective cooling of the top surface of the skin tissue, resulting in a boundary condition of third kind,

$$-k_5 \left.\frac{\partial T_5}{\partial x}\right|_{x=b_5} = h(T(b_5,y) - T_\infty) \tag{45}$$

A solution for this case may be derived using a procedure similar to Section 2.1. The only departure from Section 2.1 comes in the resistor network solution, shown in Eq. (8). In this case, $T_{j,r}(x)$ continues to be given by Eq. (11). However, due to the additional convective cooling term in the boundary condition at the top surface, the expression for Q in Eq. (12) must be modified as follows:

Table 2
Values of various parameters in the boundary conditions.

Parameter	T_{sur} (°C)	q_{sur} (W/m^2) $a/4 \leqslant y \leqslant 3a/4$	h (W/m^{2}K)	T_{bl} (°C)
Parameter values	4, 17, 40	10, 80, 200	5, 100, 500	37 [13,15]

$$Q = \frac{T_\infty - T_{bl}}{\left(\sum_{j=1}^{5} \frac{d_j}{k_j} + \frac{1}{h}\right)} \tag{46}$$

where, $d_j = b_j - b_{j-1}$, $j = 1$–5 and $b_0 = 0$

Thus, $T_{j,r}(x)$ is given by Eq. (11) where Q is replaced by Eq. (46). The rest of the solution continues to be similar to the solution previously derived for $T_{j,s}(x,y)$ in Section 2.1. A detailed derivation of this case can be found in [44].

Thus, in this section an analytical solution for temperature distribution in a two-dimensional multilayer tissue is derived. The extension of the solution to a three dimensional case is quite straightforward, but more computationally intensive, due to the introduction of double summations and double integrals.

3. Results and discussion

This section discusses temperature distribution in a five-layer skin tissue computed using the analytical models discussed in the previous section. These examples serve as tools to understand the fundamental behavior of the problem. Previously reported thermophysical property data for various skin layers are used [43]. Table 2 lists the values of parameters related to the boundary conditions analyzed here. Fig. 2(a) shows a comparison between

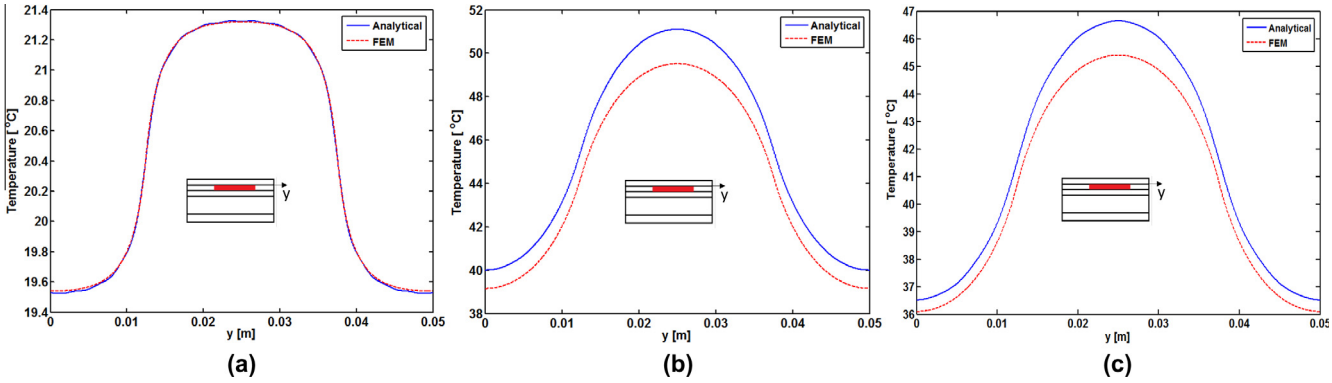

Fig. 2. Temperature distribution along the interface of papillary dermis and epidermis layer computed using the analytical model, and comparison with finite-element simulations for (a) constant temperature, (b) constant heat flux, and (c) convective heat transfer boundary conditions discussed in Section 2.

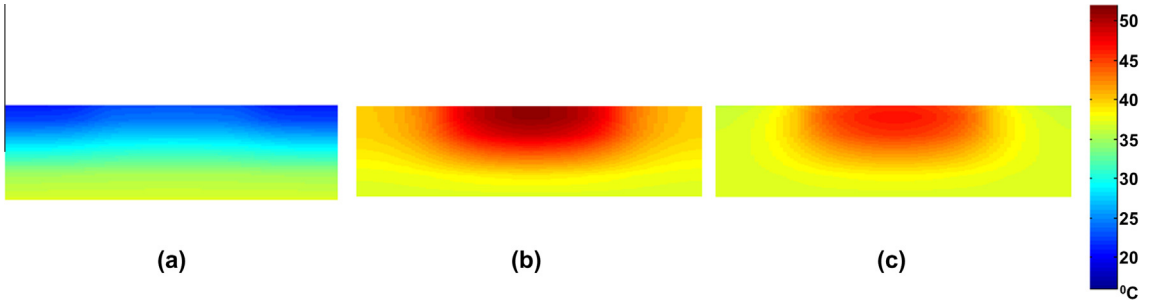

Fig. 3. Contour plots of temperature distribution in a multilayer skin tissue for (a) constant temperature, (b) constant heat flux, and (c) convective heat transfer boundary conditions discussed in Section 2.

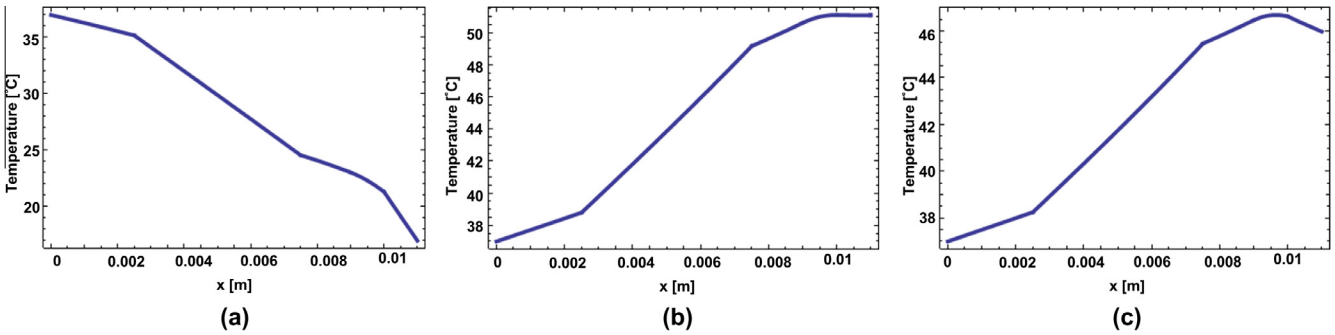

Fig. 4. Temperature distribution along the centerline ($y = a/2$) for all layers as a function of x (a) constant temperature, (b) constant heat flux, and (c) convective heat transfer boundary conditions discussed in Section 2.

the theoretical solution and a finite element simulation. Temperature at the interface of papillary dermis and epidermis layer is compared. In this case, the temperature is prescribed to be 17 °C at the top surface of the skin tissue. Note that in finite-element simulations, the $-m^2T$ term is modeled as a temperature-dependent volumetric heat sink. Grid refinement is carried out in order to ensure grid independence of the finite-element simulation results. There is good agreement between the analytical model and finite-element simulations results, with a deviation of 0.04% between the two. Similar validation against finite-element simulations is shown in Fig. 2(b) and (c) for constant heat flux and convective boundary conditions respectively at the top surface (Sections 2.2 and 2.3 respectively). In Fig. 2(b), a 10 W/m^2 heat flux is prescribed, while in Fig. 2(c), a heat transfer coefficient of 5 W/m^{2}K is assumed with an ambient temperature of 17 °C. Similar to Fig. 2(a), there is good agreement between the two in these cases. The deviation between the two occurs both due to truncation of infinite series in the model, as well as due to discretization involved in the finite-element simulations. In addition to comparison with finite-element simulations, residuals for the governing equation and boundary conditions are computed and found to be very small for each case.

Fig. 3(a)–(c) present contour plots of the entire tissue region for the three cases discussed in Section 2. Same parameters as Fig. 2 are used. These plots illustrate the temperature distribution in the cross section of tissue under study in the presence of a tumor. A peak temperature of 21.3, 51.1, and 46.7 °C is obtained for a tumor region generating 500,000 W/m^3 [8] under the three boundary conditions. Fig. 4(a)–(c) shows the variation of temperature distribution along x, the vertical direction through all layers. Note that these plots are not smooth at the intersections between layers due to the unequal thermal conductivities of the layers.

A parametric analysis is carried out to understand the effect of various geometric and bio-transport parameters, as well as boundary conditions on the temperature distribution in the multilayer structure. The effect of heat generation rate in the tumor is considered first. Fig. 5(a)–(c) show temperature plots at the interface of the papillary dermis and epidermis layer for different values of the volumetric heat generation rate in the tumor, while maintaining the tumor length at the half-length of the tissue. These figures correspond to the three boundary conditions discussed in Section 2, using the same numerical values as Fig. 2(a)–(c). Volumetric heat generation rates considered here are within the range of values reported in the past for magnetic nanoparticle based thermal therapies for cancer [8]. It is found, as expected, that the temperature at the interface increases within increasing volumetric heat generation strength. The peak temperature rise occurs along the region where the tumor is present, and tapers off outwards. Fig. 6(a)–(c) plot the temperature distribution at the same location, as a function of the tumor length for constant total heating strength. These figures correspond to the three boundary conditions discussed in Section 2. It is found that the temperature

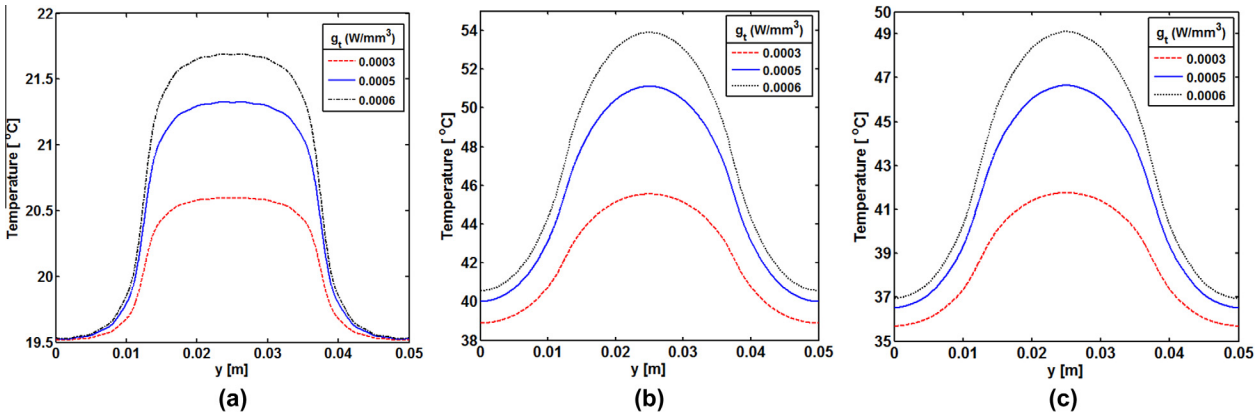

Fig. 5. Temperature distribution at the interface between papillary dermis and epidermis layer as a function of volumetric heat generation rate in the tumor for (a) constant temperature, (b) constant heat flux, and (c) convective heat transfer boundary conditions discussed in Section 2.

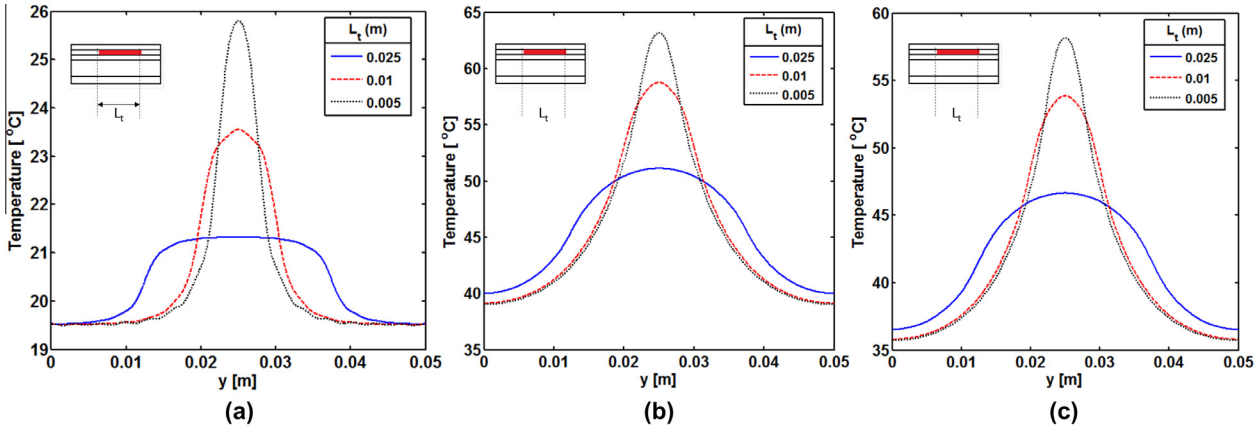

Fig. 6. Temperature distribution at the interface between papillary dermis and epidermis layer as a function of tumor size for (a) constant temperature, (b) constant heat flux, and (c) convective heat transfer boundary conditions discussed in Section 2.

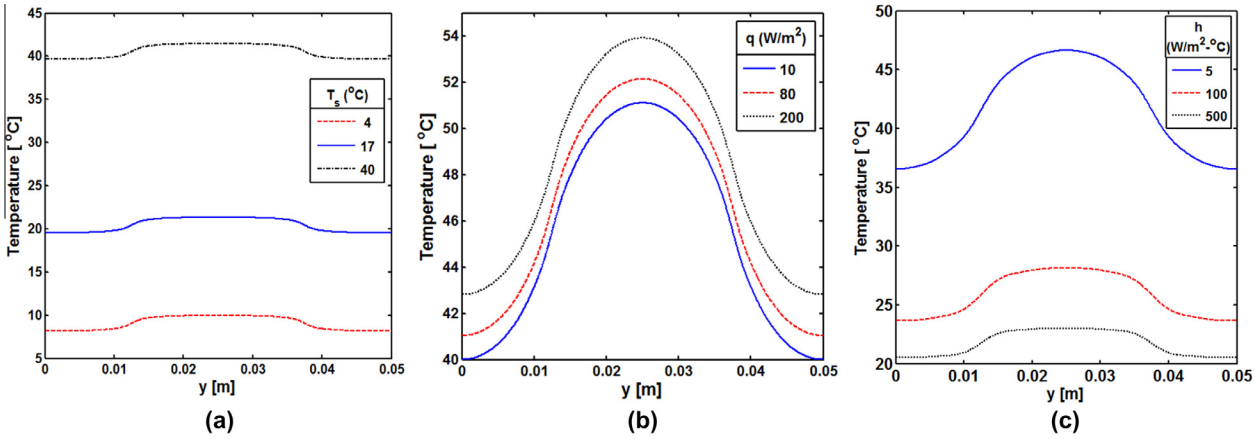

Fig. 7. Temperature distribution at the interface between papillary dermis and epidermis layer as a function of the boundary condition for (a) constant temperature, (b) constant heat flux, and (c) convective heat transfer boundary conditions discussed in Section 2.

distribution widens and the peak temperature rise reduces as the size of the tumor increases. This occurs due to the reduced volumetric heat generation as the tumor size increases. Fig. 7(a) presents the dependence of the temperature distribution on the top surface temperature for the boundary condition of the first kind. As the surface temperature at the top surface drops from 40 °C to 4 °C, a significant drop in the temperature profile at the top region of the tumor is observed. This is expected as a larger gradient is created when the value of the surface temperature is reduced. The analytical model presented in Section 2 can accurately predict the temperature around the tumor for a constant temperature applied at the surface of skin tissue and can serve as a design tool for various heating or cooling scenarios for skin tissue. Fig. 7(b) presents similar results for the boundary condition of the second kind. The tissue temperature increases with increase in the intensity of the applied heat flux. This may help in designing and regulating the heat intensity supplied by an external device during therapy. The effect of convective cooling on the top surface of skin is analyzed in Fig. 7(c) using the derived analytical solution in Section 2.3. As the value of the convective heat transfer coefficient increases, resulting in a shift from natural to forced convection, the temperature at the interface of papillary dermis and epidermis layer drops. Fig. 7(a)–(c) quantify the effect of external thermal interventions on the temperature distribution in the multilayer skin structure. Through the analytical derivation of the temperature distribution in the multilayer structure, these analyses may help the design of cooling devices for athletes [45] as well as thermal-based therapies for skin cancers.

4. Conclusion

The paper presents an analytical solution for bioheat transfer in multilayer structure such as skin. This may be of significant technological importance since several cancer treatment therapies are thermally driven, and since heating and cooling of skin is carried out for various applications. The effect of heat generation within a tumor region in the skin, as well as external boundary conditions are accounted for in the models, which are found to be in good agreement with finite-element simulations. Besides improving the theoretical understanding of bioheat transport in a multilayer structure, the results discussed here may also be useful for design of various biomedical and biomechanics related applications for both healthy and diseased tissue.

Conflict of interest

None declared.

References

[1] J.C. Chato, A view of the history of heat transfer in bioengineering, Advances in Heat Transfer, Bioengineering Heat Transfer, vol. 22, Academic Press Inc., 1948.
[2] H.H. Pennes, Analysis of tissue and arterial blood temperatures in the resting human forearm, J. Appl. Physiol. 1 (1948) 93–122.
[3] M.M. Chen, K.R. Holmes, Microvascular contributions in tissue heat transfer, Ann. New York Acad. Sci. 335 (1980) 137–150.
[4] T.C. Shih, P. Yuan, W.L. Lin, H.S. Kou, Analytical analysis of the Pennes bioheat transfer equation with sinusoidal heat flux condition on the skin surface, Med. Eng. Phys. 29 (9) (2007) 946–953, http://dx.doi.org/10.1016/j.medenghpy.2006.10.008.
[5] K.J. Chua, S.K. Chou, On the study of the freeze-thaw thermal process of a biological system, App. Therm. Eng. 29 (2009) 3696–3709.
[6] S.M. Becker, A.V. Kuznetsov, Local temperature rises influence *in vivo* electroporation pore development: a numerical stratum corneum lipid phase transition model, J. Biomech. Eng. 129 (5) (2007) 712–721, http://dx.doi.org/10.1115/1.2768380.
[7] M.A. Giordano, G. Gutierrez, C. Rinaldi, Fundamental solutions to the bioheat equation and their application to magnetic fluid hyperthermia, Int. J. Hyperthermia 26 (5) (2010) 475–484, http://dx.doi.org/10.3109/02656731003749643.
[8] A. Attaluri, R. Ma, L. Zhu, Using MicroCT imaging technique to quantify heat generation distribution induced by magnetic nanoparticles for cancer treatments, J. Heat Transfer 133 (1) (2010) 011003, http://dx.doi.org/10.1115/1.4002225.
[9] K. Wang, F. Tavakkoli, S. Wang, K. Vafai, Analysis and analytical characterization of bioheat transfer during radiofrequency ablation, J. Biomech. 48 (2015) 930–940.
[10] S. Weinbaum, L.M. Jiji, D.E. Lemmons, Theory and experiment for the effect of vascular microstructure on surface tissue heat transfer part I: anatomical foundation and model conceptualization, ASME, J. Biomech. Eng. 106 (1984) 321–330.
[11] S. Weinbaum, L.M. Jiji, D.E. Lemmons, Theory and effect of vascular microstructure on surface tissue heat transfer part II: model formulation and solution, ASME, J. Biomech. Eng. 106 (1984) 331–341.
[12] C.K. Charny, Mathematical models of bioheat transfer, Advances in Heat Transfer, Bioengineering Heat Transfer, vol. 22, Academic Press Inc., 1992.
[13] J. Liu, Bioheat transfer model, Wiley Encyclopedia of Biomedical Engineering, 2006. doi: 10.1002/9780471740360.
[14] F.A. Duck, Physical Properties of Tissue: A Comprehensive Reference Book, Academic Press Inc., 1990.
[15] Z.S. Deng, J. Liu, Analytical study on bioheat transfer problems with spatial or transient heating on skin surface or inside biological bodies, J. Biomech. Eng. 124 (6) (2002) 638–649, http://dx.doi.org/10.1115/1.1516810.
[16] S. Mahjoob, K. Vafai, Analytical characterization of heat transport through biological media incorporating hyperthermia treatment, Int. J. Heat Mass Transfer 52 (5–6) (2009) 1608–1618, http://dx.doi.org/10.1016/j.ijheatmasstransfer.2008.07.038.
[17] S. Mahjoob, K. Vafai, Analysis of bioheat transport through a dual layer biological media, J. Heat Transfer 132 (3) (2010) 031101, http://dx.doi.org/10.1115/1.4000060.

[18] K. Yue, X. Zhang, F. Yu, An analytic solution of one dimensional steady-state Pennes bioheat transfer equation in cylindrical coordinates, J. Therm. Sci. 13 (3) (2004) 255–258, http://dx.doi.org/10.1007/s11630-004-0039-y.
[19] J. Okajima, S. Maruyama, H. Takeda, A. Komiya, Dimensionless solutions and general characteristics of bioheat transfer during thermal therapy, J. Therm. Biol. 34 (8) (2009) 377–384, http://dx.doi.org/10.1016/j.jtherbio.2009.08.001.
[20] H. Askarizadeh, H. Ahmadikia, Analytical study on the transient heating of a two-dimensional skin tissue using parabolic and hyperbolic bioheat transfer equations, Appl. Math. Modell. 39 (2015) 3704–3720.
[21] L. Hu, A. Gupta, P.J. Gore, L.X. Xu, Effect of forced convection on the skin thermal expression of breast cancer, J. Biomech. Eng. 126 (2004) 204–211, http://dx.doi.org/10.1115/1.1688779.
[22] X. He, S. Mcgee, J.E. Coads, F. Schmidlin, P.A. Iaizzo, D.J. Swanlund, S. Kluge, E. Rudie, J.C. Bischoff, Investigation of thermal and tissue injury behavior in microwave thermal therapy using a procine kidney model, Int. J. Hyperthermia 20 (6) (2004) 567–593.
[23] S. Karaa, J. Zhang, A numerical study of a 3D bioheat transfer problem with different spatial heating, <www.cs.uky.edu/~jzhang/pub/REPORT/bioheat3d.pdf>.
[24] B.H. Dennis, R.C. Eberhart, G.S. Dulikravich, S.W. Radons, Finite element simulation of cooling of realistic 3-D human head and neck, J. Biomech. Eng. 125 (6) (2004) 832–840, http://dx.doi.org/10.1115/1.1634991.
[25] L. Wu, J. Cheng, W. Liu, X. Chen, Numerical analysis of electromagnetically induced heating and bioheat transfer for magnetic fluid hyperthermia, IEEE Trans. Mag. 51 (2) (2015).
[26] M.Y. Ge, K.J. Chua, M. Shu, W.M. Yang, Analytical and numerical study of tissue cryofreezing via the immersed boundary method, Int. J. Heat Mass Transfer 83 (2015) 1–10.
[27] R. Singh, K. Das, J. Okajima, S. Maruyama, S.C. Mishra, Modeling skin cooling using optical windows and cryogens during laser induced hyperthermia in a multilayer vascularized tissue, Appl. Therm. Eng. 89 (2015) 28–35.
[28] J. Crezee, J.J.W. Lagendijk, Experimental verification of bioheat transfer theories: measurement of temperature profile around large blood tissues, Phys. Med. Biol. 35 (1990) 905, http://dx.doi.org/10.1088/0031-9155/35/7/007.
[29] R. Heller, M.J. Jaroszeski, D.S. Reintgen, C.A. Puleo, R.C. DeCOnti, R.A. Gilbert, L.F. Glass, Treatment of cutaneous and subcutaneous tumors with electrochemotherapy using intralesional bleomycin, Cancer 83 (1) (1998) 148–157, http://dx.doi.org/10.1002/(SICI)1097-0142(19980701)83:1<148::AID-CNCR20>3.0.CO;2-W.
[30] A. Gothelf, M.L. Mir, J. Gehl, Electrochemotherapy: results of cancer treatment using enhanced delivery of bleomycin by electroporation, Cancer Treat. Rev. 29 (5) (2003) 371–387, http://dx.doi.org/10.1016/S0305-7372(03)00073-2.
[31] A.R. Denet, R. Vanbever, V. Preat, Skin electroporation for transdermal and tropical delivery, Adv. Drug Delivery Rev. 56 (5) (2003) 659–674, http://dx.doi.org/10.1016/j.addr.2003.10.027.
[32] U. Pliquett, Mechanistic studies of molecular transdermal transport due to skin electroporation, Adv. Drug Delivery Rev. 35 (1) (1999) 41–60, http://dx.doi.org/10.1016/S0169-409X(98)00062-3.
[33] P.M. Cetingul, Using high resolution infrared imaging to detect melanoma and dysplastic nevi (PhD. thesis), UMI Number: 3428591, ProQuest LLC, 2010.
[34] D. Yang, M.C. Converse, D.M. Mahvi, J.G. Webster, Expanding the bioheat equation to include tissue internal water evaporation during heating, IEEE Trans. Biomed. Eng. 54 (8) (2007).
[35] A. Haji-Sheikh, J.V. Beck, D. Agonafer, Steady-state heat conduction in multilayer bodies, Int. J. Heat Mass Transfer 46 (13) (2003) 2363–2379, http://dx.doi.org/10.1016/S0017-9310(02)00542-2.
[36] J. Geer, A. Desai, B. Sammakia, Heat conduction in multilayered rectangular domains, ASME J. Electron. Packag. 129 (4) (2007) 440–451, http://dx.doi.org/10.1115/1.2804094.
[37] L. Choobineh, A. Jain, Analytical solution for steady-state and transient temperature field in vertically integrated three-dimensional integrated circuits (3D ICs), IEEE Trans. Compon. Packag. Manuf. Technol. 2 (12) (2012) 2031–2039, http://dx.doi.org/10.1109/TCPMT.2012.2213820.
[38] L. Choobineh, A. Jain, An explicit analytical model for rapid computation of temperature field in a three-dimensional integrated circuit (3D IC), Int. J. Therm. Sci. 87 (2015) 103–109, http://dx.doi.org/10.1016/j.ijthermalsci.2014.08.012.
[39] C. Sturesson, S. Andersson-Engels, A mathematical model for predicting the temperature distribution in laser-induced hyperthermia. Experimental evaluation and applications, Phys. Med. Biol. 40 (1995) 2037–2052.
[40] T.L. Bergman, A.S. Lavine, F.P. Incropera, D.P. Dewitt, Fundamentals of Heat and Mass Transfer, Seventh ed., John Wiley & Sons Inc., 2011.
[41] R.V. Churchill, Fourier Series and Boundary Value Problems, McGraw-Hill Book Company Inc., 1941.
[42] N. Ozisik, Heat Conduction, Second ed., John Wiley and Sons Inc., 1980.
[43] T.Y. Cheng, C. Herman, "Optimization for skin cooling for thermographic imaging of near-surface lesions", in: Proc. of the ASME 2011 International Mechanical Engineering Congress & Exposition, IMECE2011- 65221, pp. 351–360, 2011. doi: 10.1115/IMECE2011-65221.
[44] D. Sarkar, A. Jain, A. Haji-Sheikh, "Analytical temperature distribution in a multi-layer tissue structure in the presence of a tumor", in: Proc. of the ASME 2013 International Mechanical Engineering Congress & Exposition, IMECE2013-63275, pp. V08AT09A060, 2013. doi: 10.1115/IMECE2013-63275.
[45] D.A. Grahn, H.C. Heller, Methods and devices for extracting thermal energy from the body core of a mammal, 2003, U.S. Patent, Patent No. US 6,656,208 B2.